

# On-line Characterization of YBCO Coated Conductors Using Raman Spectroscopy Methods

V. A. MARONI,\* J. L. REEVES, and G. SCHWAB

*Argonne National Laboratory, Argonne, Illinois 60439 (V.A.M.); and SuperPower, Inc., Schenectady, New York 12304 (J.L.R., G.S.)*

The use of Raman spectroscopy for on-line monitoring of the production of superconducting  $\text{YBa}_2\text{Cu}_3\text{O}_{6+x}$  (YBCO) thin films on long-length metal tapes coated with textured buffer layers is reported for the first time. A methodology is described for obtaining Raman spectra of YBCO on moving tape exiting a metal-organic-chemical-vapor-deposition (MOCVD) enclosure. After baseline correction, the spectra recorded in this way show the expected phonons of the specific YBCO crystal orientation required for high supercurrent transport, as well as phonons of non-superconducting second-phase impurities when present. It is also possible to distinguish YBCO films that are properly textured from films having domains of misoriented YBCO grains. An investigation of the need for focus control on moving tape indicated that focusing of the laser on the surface of the highly reflective YBCO films exiting the MOCVD enclosure tends to produce aberrant photon bursts that swamp the Raman spectrum. These photon bursts are very likely a consequence of optical speckle effects induced by a combination of surface roughness, crystallographic texture, and/or local strain within the small grain microstructure of the YBCO film. Maintaining a slightly out-of-focus condition provides the best signal-to-noise ratio in terms of the obtained Raman spectra. In addition to examining moving tape at the post-MOCVD stage, Raman spectra of the film surface can also be recorded after the oxygen anneal performed to bring the YBCO to the optimum superconducting state. Consideration is given to data processing methods that could be adapted to the on-line Raman spectra to allow the tagging of out-of-specification tape segments and, at a more advanced level, feedback control to the MOCVD process.

Index Headings: Raman; Superconductor; On-line monitoring; Optical speckle.

## INTRODUCTION

The discovery of high-critical-temperature superconductivity (HTS) in a particular class of cuprate ceramics in 1986 by Bednorz and Müller<sup>1</sup> and the bevy of subsequent discoveries of elevated temperature superconductivity in oxide<sup>2</sup> and boride<sup>3</sup> materials set off a worldwide quest to develop and commercialize superconductor-based products for the electric power, medical, and communications markets, to name but a few.<sup>4</sup> The principal objective of this worldwide quest is the development of methods to fabricate and deploy functionally reliable, economically tenable HTS embodiments for transmitting, transforming, generating, conditioning, and storing electrical energy. Research activities are focused on improving the electrical performance properties of HTS materials through the elucidation, manipulation, and control of processing pathways and the development of practical methods for mass-producing commercial conductors. At the present time,  $\text{YBa}_2\text{Cu}_3\text{O}_{6+x}$  (YBCO) in thin film form deposited on long lengths of textured/buffered metal substrate is the leading candidate for large-scale commercialization of HTS systems.<sup>5</sup> The industry is

focused on high-yield volume production of YBCO coated conductor, in long (~1000 m) lengths with uniform properties. The capability to mass-produce contiguous kilometer lengths of high-performance conductor will require advances in process equipment and process control. In particular, the development of on-line process monitoring tools, particularly ones that can provide timely feedback to the process control system to compensate/correct for off-normal or out-of-specification conditions, will be very valuable. Even at a minimum level of on-line monitoring, instrumentation that “tags” out-of-specification tape segments for subsequent excision and splicing could be beneficial for efficient production operations.

One of the tools currently under investigation for monitoring the direct deposition of YBCO films in an on-line mode is Raman spectroscopy. The interpretation of the Raman spectra of YBCO for practical applications and the adaptation of Raman spectroscopy to YBCO coated conductor tapes in a production type (reel-to-reel) environment were reviewed and discussed in two prior publications.<sup>6,7</sup> In this paper, we present results of the first known attempts to employ Raman spectroscopy as an on-line monitor of the quality of epitaxial YBCO thin films deposited on long-length metal substrates coated with textured buffer layers.<sup>8,9</sup> These measurements were performed on YBCO coated conductor exiting a metal-organic-chemical-vapor-deposition (MOCVD) chamber on a 300-meter-plus capacity tape manufacturing line at SuperPower, Inc.<sup>8</sup>

## EXPERIMENTAL

The process technology employed by SuperPower, Inc. to produce MOCVD YBCO coated conductor in 100+ meter lengths has been described elsewhere.<sup>8</sup> The texturing approach used in this manufacturing operation is based on ion beam assisted deposition (IBAD) of an epitaxial template layer (e.g., MgO) on the metal substrate surface. The principles of IBAD-based coated conductor texturing have been reviewed by Arendt et al.<sup>9</sup> The equipment used for on-line Raman measurements consisted of a fiber-optic probe attached to a Kaiser Optical Systems, Inc. (KOSI) RamanRxn1™ spectrometer. Raman excitation was produced using an Invictus 785 nm near-infrared GaAlAs diode laser operated such that a nominal power level of 150–200 mW was delivered to an approximately 60  $\mu\text{m}$  spot. The configuration used to make on-line measurements is pictured in Fig. 1. The Raman probe and the antechamber to which it is attached are circled in the picture. The large enclosure to the left of the antechamber houses the MOCVD equipment used to deposit the YBCO films. The round chamber to the right of the antechamber encloses the reel that takes up the coated tape.

For purposes of comparison and clarification, a series of off-line Raman microspectroscopic measurements was made using

Received 20 September 2006; accepted 5 February 2007.

\* Author to whom correspondence should be sent. E-mail: maroni@cmt.anl.gov.

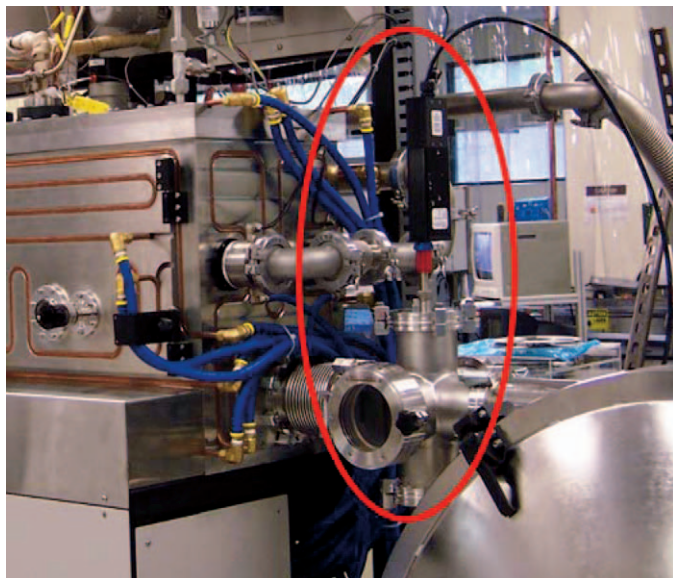


FIG. 1. Photograph showing the on-line configuration of the Raman probe used in conjunction with SuperPower's MOCVD processing chamber.

a Renishaw RM2000 imaging Raman microscope equipped with a 633 nm HeNe laser. The methodology for interrogating small specimens of coated conductor (approximately 1 cm × 1 cm) and long-length tape by Raman microscopy using the RM2000 has been described in considerable detail in two prior publications.<sup>6,7</sup>

## RESULTS AND DISCUSSION

**Characterization of the On-line Raman Probe.** One of the novelties of the approach used in this adaptation of Raman spectroscopy to on-line monitoring of YBCO deposition is that the Raman spectra are collected on moving tape in a static grating mode, using the charge-coupled device (CCD) detector as the monochromator. Therefore, as the tape moves under the optical element that concurrently focuses the laser on the tape surface and collects the Raman scattered radiation from the YBCO film, an average Raman spectrum is collected for a fixed length of tape. For the measurements on moving tapes reported in this paper, the tape travel speed was 10 m/h or approximately 17 cm/min. The spectrometer was set for a data acquisition period of 5 seconds in intervals of 1 minute. Thus, each of the stored, moving tape spectra constitutes an average spectrum of an approximately 1.4 cm segment out of each 17 cm length passing the probe head. (This intermittent sampling was done to limit the data files for the long lengths of tape that were examined during method development and testing.) KOSI's HoloGRAMS™ software controlled the spectrometer, as well as the data acquisition and export.

The focal length of the collection optic at the tip of the probe is 11 mm and no attempt has yet been made to maintain a specific focus level on moving tape segments. Nonetheless, the spectral quality and reproducibility achieved thus far have been of sufficiently high quality to provide useful information. The vast majority of spectra exhibit the same peak and baseline count levels and the same overall spectral features, but on occasion random aberrant spectra are recorded.

Figure 2 shows ten spectra from a set of eleven consecutive spectra that are representative of the quality, character, and

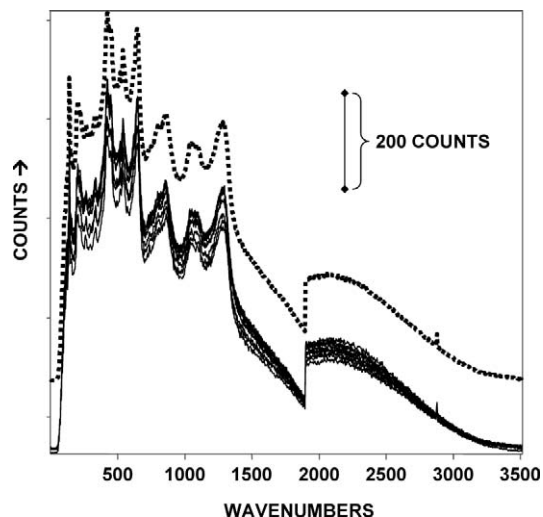


FIG. 2. Overlay of ten Raman spectra collected on a moving tape segment of MOCVD YBCO conductor (solid traces). The dotted trace is the average of the ten spectra; note that it is displaced upwards for ease of viewing. An absolute count range indicator is shown in the figure.

reproducibility of unprocessed spectra taken on moving post-MOCVD YBCO tapes. The upwardly displaced, dotted spectrum in Fig. 2 is the average of the ten "normal" spectra plotted below it. One of the eleven spectra (not shown in Fig. 2) exhibited a significantly different count range from the other ten. This aberrant spectrum is plotted in Fig. 3 together with the average "normal" spectrum from Fig. 2. In virtually all cases, the aberrant spectra show evidence of an underlying burst of photons that significantly raises the background count level without any evidence of comparable enhancement in the Raman scattering features, i.e., between 100 and 1600  $\text{cm}^{-1}$ . During data processing, the aberrant spectra are easily recognized and separated from the normal spectra when examining and interpreting the Raman features. Several likely causes for the random/occasional aberrant spectra are addressed further on in this paper. However, it is important to note that the aberrant spectral effects observed with the

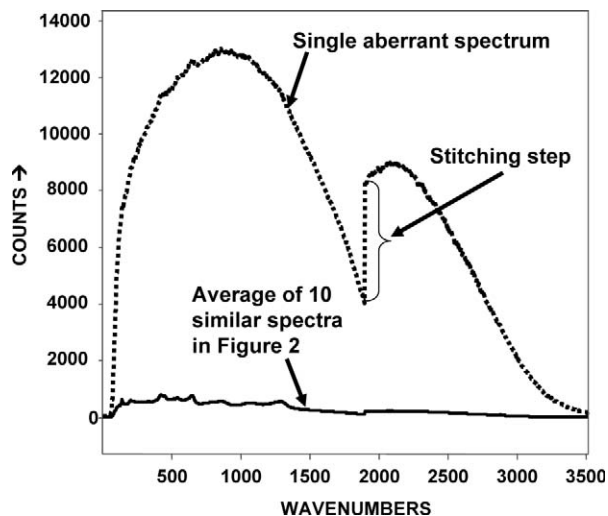


FIG. 3. The top trace shows the aberrant spectrum described in the text. The bottom trace is the average spectrum in Fig. 2 plotted on the same intensity scale.

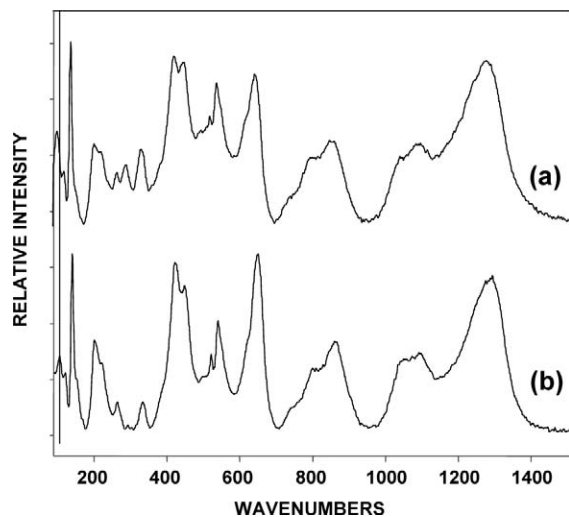


FIG. 4. (a) A typical Raman spectrum of the YBCO film exiting the MOCVD chamber. (b) Spectrum obtained by down-scaling and subtracting the aberrant spectrum in Fig. 3 from the average spectrum in Fig. 3.

KOSI spectrometer, on-line fiber-optic probe, and 785 nm excitation laser are not experienced when the same samples are examined using the Renishaw RM2000 with 633 nm excitation.

The jump in counts near  $1900\text{ cm}^{-1}$  seen in Figs. 2 and 3 is a consequence of the KOSI spectrometer's dual grating system. The instrument collects the full range Raman spectrum in two sub-ranges and stitches them together to form a single spectrum. The stitch step has turned out to be a useful artifact for baseline correction, as described below.

When "normal" spectra, such as those shown in Fig. 2, are baseline corrected and smoothed (using GRAMS/AI software), they typically appear as shown in Fig. 4a. Figure 4b was obtained by the following subtractive procedure: The count range of the spectral stitching step in the aberrant spectrum from Fig. 3 was down-scaled to match the count range of the stitch step for the average spectrum of the 10 "normal" scans in Fig. 2 and then subtracted from the average spectrum of the "normal" scans—Fig. 4a. After such treatment, the count ranges and spectral features of the two spectra in Fig. 4 come out to be much the same, as can be seen in Fig. 4. It is worthy of note that the downscaling factor required to reduce the stitch step of aberrant spectra to the range of the normal spectra stitch step is typically well over an order of magnitude. The implication of the result shown in Fig. 4 is that the Raman scattering is not increased by the scattering process that causes the background photon burst in aberrant spectra. If it were, one would expect the result of the downscaling and subtraction procedure that gave Fig. 4b to produce a near-to-null spectrum. The point here is that there seems to be no measurable additional Raman spectral intensity in the aberrant scans as compared to the normal scans. Furthermore, the down-scaled aberrant spectra provide an easily obtained/effective background corrector for the "normal" spectra.

In the interpretation of MOCVD product Raman spectra, like those shown in Fig. 4, the useful spectral region that includes the characteristic phonons of YBCO and common impurity phases (e.g., CuO,  $\text{Y}_2\text{BaCuO}_5$ ,  $\text{BaCuO}_2$ , and  $\text{BaCO}_3$ ) is between  $100$  and  $1600\text{ cm}^{-1}$ ; hence, the description of the observed spectra will center on that spectral region. A typical

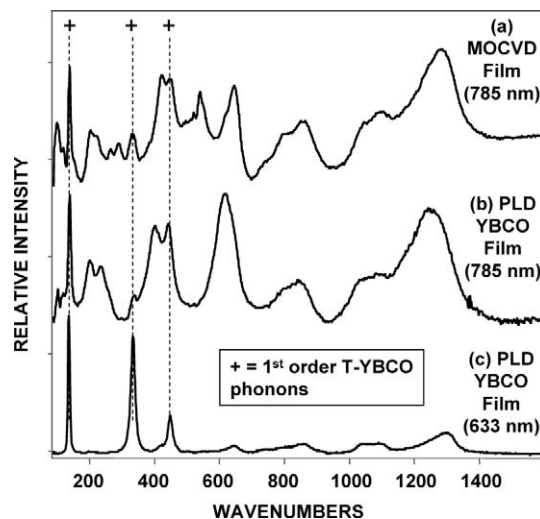


FIG. 5. (a) A representative Raman spectrum of good quality YBCO films exiting the MOCVD chamber (taken with 785 nm excitation). (b) Raman spectrum of pulse-laser-deposited (PLD) T-YBCO on a single crystal substrate excited with the 785 nm laser. (c) Raman spectrum of the same PLD T-YBCO sample excited with a 633 nm laser.

baseline-corrected spectrum of good quality MOCVD product YBCO is shown as Fig. 5a. Under the conditions used to produce these MOCVD YBCO films, the YBCO exiting the deposition chamber is under-doped in oxygen and forms in what is known as the non-superconducting tetragonal phase<sup>6</sup> for which the value of  $x$  in  $\text{YBa}_2\text{Cu}_3\text{O}_{6+x}$  is close to zero. The 785 nm excited Raman spectrum of a similarly doped, pulsed-laser-deposited (PLD) YBCO film on a high-quality single crystal substrate is shown in Fig. 5b. (This spectrum can be looked upon as a reference spectrum for high-purity, well-textured, tetragonal YBCO using 785 nm excitation.) Figure 5c is a 633 nm excited Raman spectrum of the same PLD film. Two aspects of these spectra are noteworthy. (1) The spectra of the moving MOCVD film and the static PLD film (both excited with the 785 nm laser in use at SuperPower) are very much the same. (2) Comparison of the spectra of the PLD film taken with the two different excitation wavelengths indicates that the character of the excitation process is wavelength dependent.

The spectra in Figs. 6a and 6b are averaged moving-tape spectra from two MOCVD runs conducted several months apart that produced high-performance HTS conductor. We include them here to show the consistency of the post-MOCVD spectral features from run to run. (Note that the spectrum shown in Fig. 6b is the same one shown in Fig. 5a.) After the MOCVD step, the tape is coated with a silver cap layer and subjected to an oxygen annealing treatment to transform the tetragonal YBCO (T-YBCO) to the superconducting orthorhombic form (O-YBCO) for which the value of  $x$  in  $\text{YBa}_2\text{Cu}_3\text{O}_{6+x}$  is close to 1. A typical Raman spectrum of the oxygen annealed tape after removal of the Ag cap layer (using a chemical etching process) is shown in Fig. 6c. After oxygen annealing, many of the spectral features seen in the as-deposited MOCVD YBCO spectra disappear almost completely. In particular, the features filled in with cross-hatching in Fig. 6a are for the most part absent in the top spectrum. These features are understood to arise from multi-phonon scattering emanating from T-YBCO.<sup>10,11</sup> T-YBCO is an anti-ferromagnetic insulator and this second-order scattering is due to a

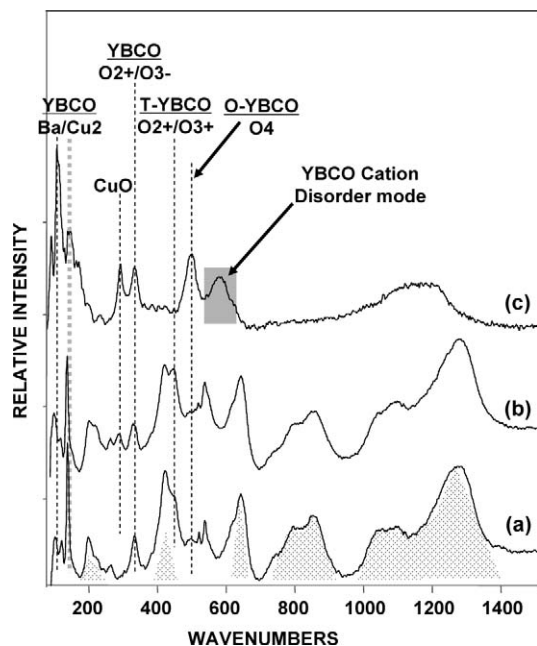


FIG. 6. (a, b) Representative Raman spectra of good quality YBCO films from the MOCVD chamber taken several months apart. (c) A representative spectrum of MOCVD-produced T-YBCO after oxygen anneal to produce the superconducting O-YBCO.

coupling effect associated with the relative closeness of the Raman excitation line energy to the charge transfer gap (CTG) in T-YBCO. It happens that the 785 nm (1.59 eV) line is considerably closer to this gap than the 633 nm (1.97 eV) line, which explains why the multi-phonon scattering effect is stronger (relative to the first-order YBCO Raman scattering) for the 785 nm line than for the 633 nm line. Figure 1 of the paper by Blumberg et al.<sup>10</sup> provides a clear illustration of this effect. The spacing between the cross-hatched bands in the bottom spectrum of Fig. 6 appears to have a value slightly over 200  $\text{cm}^{-1}$ . This observation is helpful in the interpretation of first-order spectral features around 200, 400, and 600  $\text{cm}^{-1}$ .

Most of the prominent features below 700  $\text{cm}^{-1}$  in the spectra included in Fig. 6 can be assigned to O-YBCO or T-YBCO, as indicated in the figure. The basis for these assignments is explained in a prior publication.<sup>6</sup> In summary (for the benefit of the reader), the character of the Raman spectrum of oriented YBCO grains depends on the orientation of the polarization vector of the excitation laser with respect to the crystallographic axes of the YBCO. A properly textured YBCO film on an IBAD-type coated conductor forms with the YBCO *c* axis perpendicular to the tape surface. When the excitation laser is also introduced perpendicular to the tape surface, as in this study, three of the five Raman active *c*-axis phonons of O-YBCO typically appear with moderate intensity.<sup>6</sup> They are (1) the barium mode (Ba) around 110  $\text{cm}^{-1}$ , (2) the copper-2 mode (Cu2) between 140 and 150  $\text{cm}^{-1}$  depending on the oxygen doping level, and (3) the out-of-phase centro-symmetric mode (O2+/O3-) around 340  $\text{cm}^{-1}$  involving the oxygen atoms in the Cu-O planes that actually carry the supercurrent. For T-YBCO, the Ba mode is considerably lower in intensity than the Cu2 mode but gains intensity relative to the Cu2 mode as the oxygen doping level is increased towards O-YBCO. The in-phase centro-symmetric mode (O2+/O3+), appearing at 450  $\text{cm}^{-1}$  with moderate

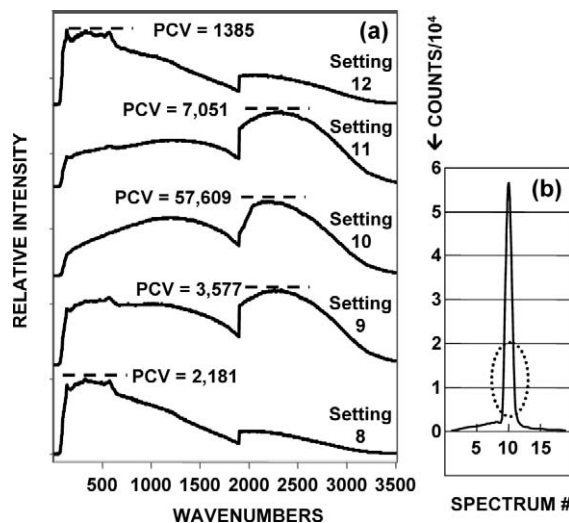


FIG. 7. (a) Selected Raman spectra from the focal position study described in the text. (b) Curve fit to the peak count values (PCVs) for each of the 19 Raman spectra from the focal position study.

intensity for T-YBCO, loses intensity relative to O2+/O3- and shifts to lower frequency (towards 435  $\text{cm}^{-1}$ ) as the oxygen doping level is increased towards O-YBCO. The fifth Raman active *c*-axis phonon is the O4 mode, which increases in frequency from 475 to 502  $\text{cm}^{-1}$  with increased oxygen doping. This mode should not appear for the excitation/collection geometry (E/CG) employed in this study (i.e., laser propagation direction parallel to the YBCO *c*-axis<sup>6</sup>) if the YBCO is well textured, meaning that there are relatively few YBCO grains with tilted *c* axes. Conversely, the appearance of the O4 mode in said E/CG provides an indication that the film has domains of tilted YBCO grains, a condition that tends to diminish transport current properties.

This knowledge of the effect of orientation and oxygen stoichiometry on the frequency and relative intensity of the YBCO phonons can be used to gain substantive information about YBCO texture quality and orthorhombic/tetragonal phase separation along the lines described in prior publications.<sup>6,7</sup> In addition, variations in the phase chemistry of the YBCO film in the post-MOCVD and post-oxygen-anneal states can be monitored over long lengths.

**Application of the On-line Raman Probe.** Our efforts to adapt the Raman probe for on-line duty in SuperPower's MOCVD manufacturing lines have required that we investigate several functional features of the probe's performance with moving tape. Because the tape is in tension during reel-to-reel MOCVD, vertical displacements of the tape perpendicular to the tape length direction tend to be small. Nonetheless, a focal point variation study was performed to determine the consequences of tape motion along the axis of the collection optic. In this study the Raman probe head was attached to a vertical positioning control and focused on a segment of static post-MOCVD YBCO tape. The laser was focused on the YBCO surface, a spectrum was taken, and thereafter, spectra were taken at 60  $\mu\text{m}$  increments along the focal axis (nine above the focal point and nine below the focal point). Representative spectra from the nineteen measurements are shown in Fig. 7a. The peak count value (PCV) is listed above each spectrum in Fig. 7a, i.e., at the position of the respective dashed lines. For the series of spectra taken, setting 10

corresponds to the laser being in focus on the YBCO film surface (hereafter referred to as the focal setting). Spectrum 8 is representative in appearance of spectra 1 through 8; and spectrum 12 is representative in appearance of spectra 12 through 19. At setting 10 and at the two adjacent settings (one focused 60  $\mu\text{m}$  above the YBCO surface and the other 60  $\mu\text{m}$  below the YBCO surface), the PCV is much higher than for subsequent spectra in either direction away from the focal setting, and the spectrum shows evidence of a background photon burst similar to that exhibited by the aberrant spectrum in Fig. 3.

Figure 7b is a fitted plot of the PCV value as a function of focal point location with respect to the "focal setting". The results in this inset suggest that the background photon bursts are caused or perhaps exacerbated by having the excitation laser focused on the YBCO surface. This is not surprising because the surface of the YBCO film exiting the MOCVD chamber is typically highly reflective, and it is possible that focusing of the coherent laser beam on the fine grained/textured YBCO surface maximizes the reflected laser photon flux collected by the probe lens. Similar focusing tests done using a 50 $\times$ , 0.3 mm focal length optic on the Renishaw System 2000 confocal Raman microprobe did not produce a comparable aberrant spectral effect. It seems, therefore, that the aberrant spectrum effect may be associated with some feature(s) of the KOSI fiber-optic probe and spectrometer.

There are a number of possible explanations for the photon bursts in moving tape situations that need further study, including tape tilting (i.e., tilting that sends reflected white light into the collection optic), fluorescence, and the occurrence of periodic, non-specific, highly reflective defects. Also, there is a distinct possibility that optical speckle from the focused, coherent 785 nm line of the KOSI laser could be contributing to the apparent photon bursts. Optical speckle measurement and analysis techniques have been used to detect strain,<sup>12,13</sup> texturing effects,<sup>14-16</sup> and surface roughness.<sup>17,18</sup> While the investigation of such possibilities for MOCVD YBCO tape monitoring is beyond the scope of this manuscript, there is ample incentive to pursue the diagnostic potential of optical speckle measurements in connection with the development of on-line Raman methods for the MOCVD process.

A pivotal technical issue in YBCO coated conductor development has been the achievement of high through-thickness supercurrent transport. Typically, as the YBCO film is made thicker and thicker in single pass depositions, the overall critical current density (in amperes/cm<sup>2</sup> of YBCO) drops off monotonically with increasing thickness, indicating that the YBCO quality is degrading with increasing thickness. One of the solutions to this problem under study at SuperPower is to deposit thick YBCO films by multiple passes instead of in a single pass, e.g., by depositing three individual 0.5  $\mu\text{m}$  layers of YBCO in three consecutive passes through the MOCVD chamber, rather than depositing one 1.5  $\mu\text{m}$  layer in a single pass. In one such three-pass run, the Raman probe was used to monitor the spectral character during each pass. Two characteristics were tracked in this study: (1) the total integrated count level for each individual spectrum, and (2) the information in the extracted Raman spectra concerning phase composition and film orientation. During this series of measurements, an attempt was made to maintain positional registry, such that the Raman probe data at a given tape position could be compared on a layer-to-layer basis.

A graphical representation of the total integrated counts (linear scale) for each spectrum taken during each pass is presented in Fig. 8. Here, the graphs for each pass are stacked one above the other to allow a comparison of the number and pass-to-pass location of photon bursts. Examination of these graphs shows that the pattern of bursts is random. A plot of the integrated counts (logarithmic scale) for each spectrum taken during each of the three passes over an approximately two-meter length of a 100-meter long tape is shown in Fig. 9. In this plot we observe again that the photon bursts are random (i.e., they show no correspondence to a particular tape position). We also observed small periodic dips in the non-burst integrated count values that are marked with arrows in Fig. 9. The dips seem to be in positional registry for pass 2 and pass 3 but not so for pass 1, although the spacing of the dips appears to be the same for all three passes. We know that this mis-registry between pass 1 and passes 2 and 3 is due to having inadvertently started the Raman data acquisitions for passes 2 and 3 at a different place from the start of pass 1. The cause of the dips is still under investigation, but it is believed to be related to a process parameter fluctuation.

An evaluation has been made of the Raman spectra extracted from the non-burst spectra in Fig. 9 and in spectra from other comparable long-length MOCVD tape production runs. Typically, the Raman spectra of post-MOCVD and oxygen annealed product tape closely resemble those shown in Fig. 5. We refer to these as the characteristic or optimum Raman spectra of post-MOCVD and post anneal tape. Occasionally, we obtain spectra from low performing tape segments that are different from those in Fig. 5. Examples of post-MOCVD spectra that correlate with optimum performance, near-to-optimum performance, and two levels of below-optimum performance are presented in Fig. 10. We are currently trying to connect the spectral differences to specific compositional and/or microstructural abnormalities in the post-MOCVD and fully processed YBCO tapes and to further connect these abnormalities with electrical performance of the finished tape. Assuming these connections can be demonstrated, it should be possible to develop a Raman based tool for tagging out-of-specification tape segments that can subsequently be repaired or excised.

Taking a more advanced view of the process monitoring possibilities, the relative intensities at a series of test point frequencies, such as the set of 15 indicated in Fig. 10, could serve as the basis for feedback signaling to the MOCVD control system that process parameter adjustments are needed. For example, down-scaling of a nearby aberrant spectrum could be done to create a baseline corrected spectrum (as illustrated in Fig. 4). Next, the count values at test points 2, 4, 7, 10, 12, and 15 could be used (in whole or in part) to cross check the aforementioned background correction. Count values at test points 1, 6, and 9, the peak frequencies for the three most prominent first-order Raman phonons of T-YBCO, could be used to gauge the relative T-YBCO content. Count values at test points 3, 8, and 14, the peak frequencies of the multi-phonon T-YBCO scattering below 700  $\text{cm}^{-1}$ , also provide a gauge of the T-YBCO content and oxygen stoichiometry. The intensities at test points 5, 11, and 13 relative to intensities at other points could be used to gauge (1) the relative content of certain second phases that occur with regularity in off-stoichiometric product (e.g., CuO and

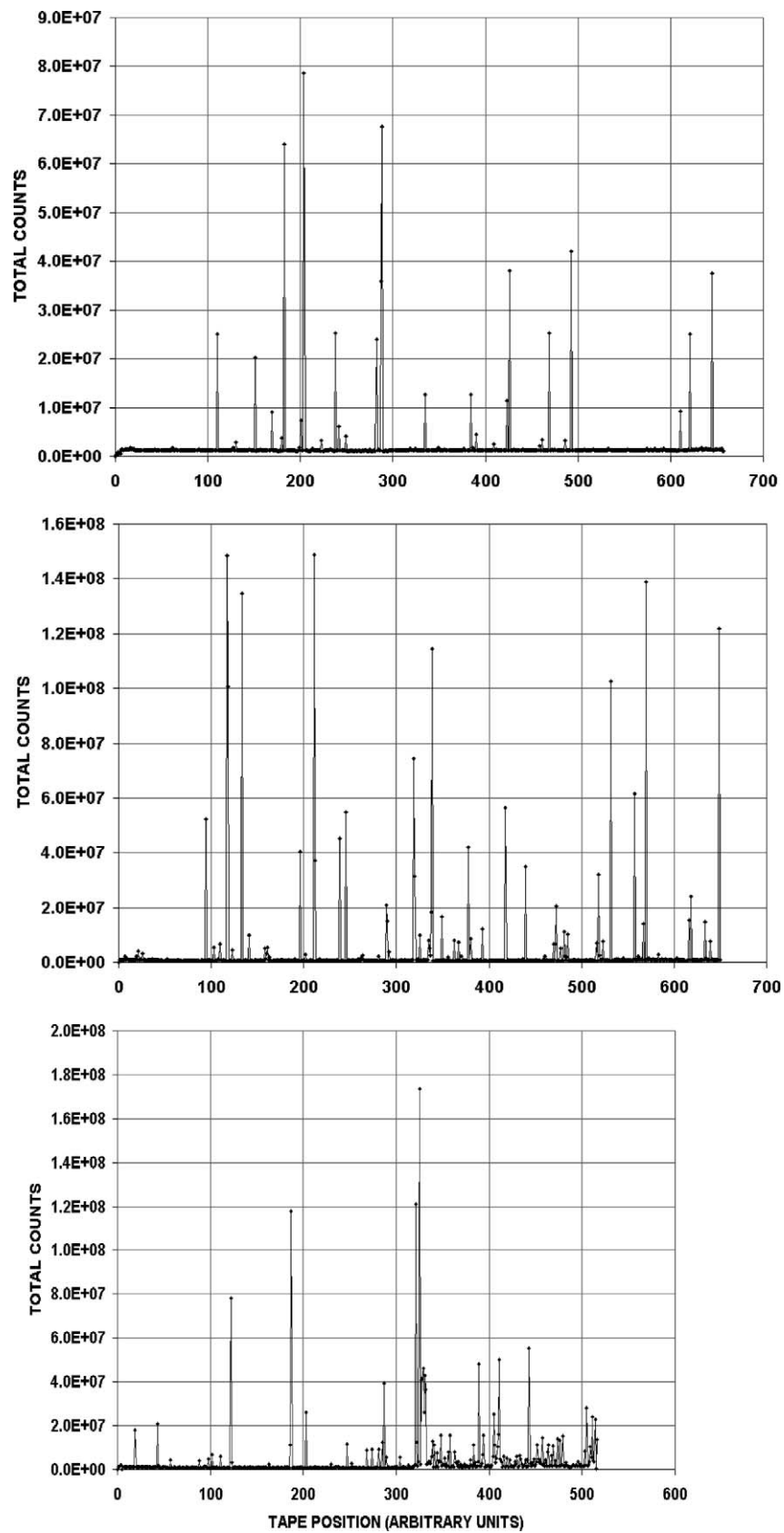


FIG. 8. Total integrated count values for a 100 meter tape subjected to a three-pass YBCO deposition. (**Top**) first, (**middle**) second, and (**bottom**) third pass.

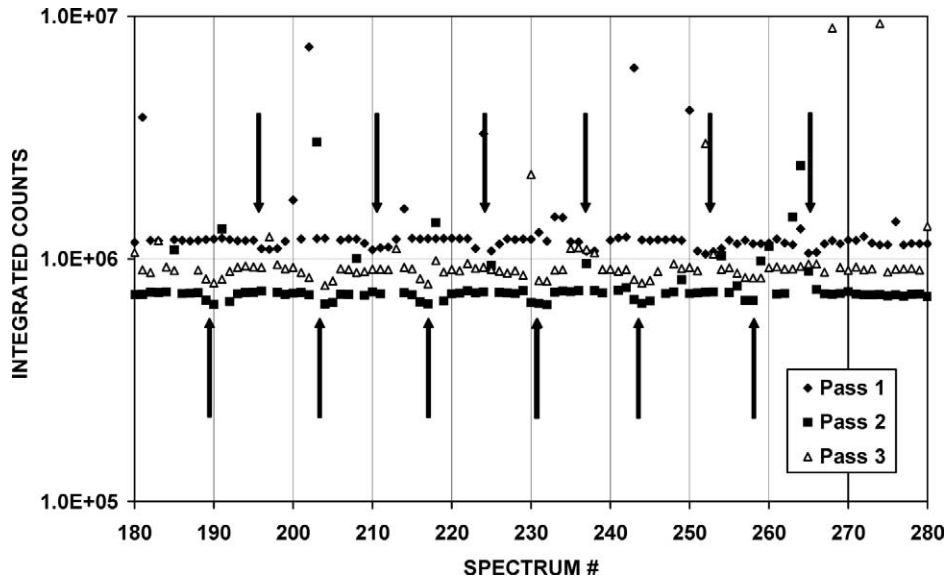


FIG. 9. Integrated count data for sequential spectra taken over a 2 meter segment of a 100 meter long tape plotted on a log scale to highlight how the total counts reveal certain types of periodicities in the MOCVD process as described in the text.

barium cuprates) and (2) the relative amount of cation disorder in the T-YBCO.<sup>6</sup>

In addition to tracking the composition of the post-MOCVD YBCO in a long-length mode, it is also possible to make reel-to-reel examinations of the oxygen annealed final product (the O-YBCO) and to correlate the O-YBCO spectral characteristics with the local critical current capacity of the conductor. Raman spectra recorded at three locations along a fully processed long-length coated conductor tape exhibiting a wide range of local critical current values,  $I_c$  in amperes (for a standard one centimeter wide tape), are plotted in Fig. 11. The results show a correlation between decreasing CuO content and increasing  $I_c$ . There is also a variation in the relative intensity of the O-YBCO O4 mode (the mode whose presence provides an indication of the extent of tilted YBCO grain development), but this does not appear to have a significant negative influence on the  $I_c$  values of single layer (i.e., single pass) films. However, the next deposition pass might be

adversely affected by a pre-existing first-pass surface covered with a significant number of tilted YBCO grains, so post-MOCVD monitoring of individual passes by Raman spectroscopy could be useful in determining prospects for successful application of additional YBCO layers.

Figure 11a is presently considered to represent the characteristic 200 to 650  $\text{cm}^{-1}$  spectrum for high performing, fully processed YBCO films prepared by the MOCVD route. Clearly, there are significant spectral differences among the three traces in Fig. 11 that accompany the differences in performance. The multiple test point approach described above in connection with the spectra in Fig. 10 could also be applied to the spectra of fully processed MOCVD films, such as those in Fig. 11.

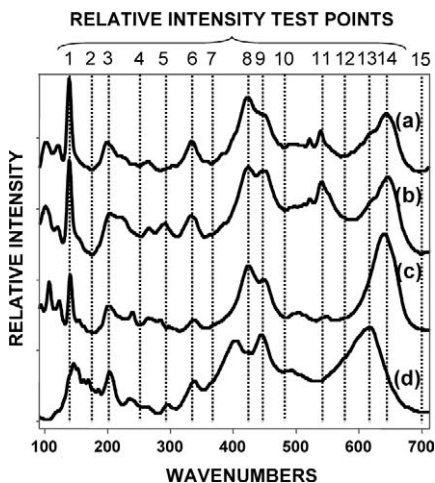


FIG. 10. (a) Optimum spectrum for as-deposited MOCVD YBCO. (b) Near to optimum, (c) further from optimum, and (d) far from optimum MOCVD YBCO.

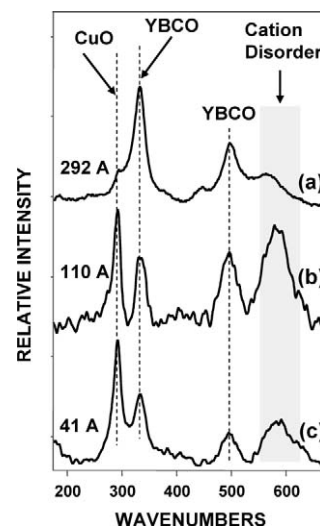


FIG. 11. (a, b, c) Traces showing a portion of the Raman spectra of fully processed MOCVD YBCO tapes that performed at varying levels in terms of critical current per centimeter width of superconductor as indicated next to each trace (A = amperes). Note that the critical current values increase with decreasing CuO content.

## CONCLUSION

The utility of Raman spectroscopy for on-line monitoring of the production of superconducting  $\text{YBa}_2\text{Cu}_3\text{O}_{6+x}$  (YBCO) thin films on long-length metal tapes has been demonstrated. Raman spectra of sufficiently high quality for YBCO composition analysis were recorded on moving tape exiting a metal-organic-chemical-vapor-deposition (MOCVD) enclosure. Baseline corrected spectra recorded in this way show the expected phonons of the specific YBCO crystal orientation required for high supercurrent transport, as well as phonons of non-superconducting second-phase impurities when present. It is also possible to distinguish YBCO films that are properly textured from films having domains of misoriented YBCO grains. Maintaining a slightly out-of-focus condition provides the best signal-to-noise ratio in the obtained Raman spectra. In addition to examining moving tape at the post-MOCVD stage, it is also possible to measure Raman spectra of the same tape after the oxygen anneal is performed to bring the YBCO to the optimum superconducting state. There appear to be promising formats for data processing that could be adapted to the on-line Raman spectra to allow the tagging of out-of-specification tape segments and feedback control to the MOCVD process. Periodic aberrant spectra observed with the on-line Raman setup employing 785 nm excitation and a fiber-optic probe may be related to optical speckle effects that require further study to determine their cause and their possible diagnostic utility. It is noteworthy that such aberrant spectral effects were not observed in examinations of the same samples using a Raman microprobe equipped with a 633 nm laser.

## ACKNOWLEDGMENTS

Research done at the Argonne National Laboratory was sponsored by the U.S. Department of Energy (DOE), Office of Electricity Delivery and Energy Reliability, as part of a DOE program to develop electric power technology,

under contract DE-AC02-06CH11357 between UChicago Argonne, LLC and the DOE. The submitted manuscript has been created by UChicago Argonne, LLC, Operator of Argonne National Laboratory ("Argonne"). Argonne is a U.S. Department of Energy Office of Science laboratory. The U.S. Government retains for itself, and others acting on its behalf, a paid-up nonexclusive, irrevocable worldwide license in said article to reproduce, prepare derivative works, distribute copies to the public, and perform publicly and display publicly, by or on behalf of the Government.

1. J. G. Bednorz and K. H. Müller, *Z. Phys. B* **64**, 189 (1986).
2. R. J. Cava, *J. Am. Ceram. Soc.* **83**, 5 (2000).
3. J. Akimitsu and T. Muranaka, *Phys. C* **388–389**, 98 (2003).
4. A. P. Malozemoff, J. Mannhart, and D. Scalapino, *Physics Today* (April 2005), pp. 41–47.
5. M. P. Paranthaman and T. Izumi, *Mater. Res. Soc. Bull.* **29**, 533 (2004), and the series of papers in the same issue that follow this overview.
6. K. Venkataraman, R. Baurceanu, and V.A. Maroni, *Appl. Spectrosc.* **59**, 639 (2005).
7. K. Venkataraman, D. F. Lee, K. Leonard, L. Heatherly, S. Cook, M. Paranthaman, M. Mika, and V. A. Maroni, *Supercond. Sci. Technol.* **17**, 739 (2004).
8. V. Selvamanickam, Y. Xie, J. Reeves, and Y. Chen, *Mater. Res. Soc. Bull.* **29**, 579 (2004).
9. P. N. Arendt and S. R. Foltyn, *Mater. Res. Soc. Bull.* **29**, 543 (2004).
10. G. Blumberg, P. Abbamonte, M. V. Klein, W. C. Lee, G. M. Ginsberg, L. L. Miller, and A. Zibold, *Phys. Rev. B* **53**, R11930 (1996).
11. V. Denisov, C. Taliani, A. G. Mal'shukov, V. M. Burlakov, E. Schönherr, and G. Ruani, *Phys. Rev. B* **48**, 16714 (1993).
12. Z. Zhang and F. Ansari, *Sens. Actuators, A* **126**, 107 (2006).
13. S. C. Schneider, B. Zagar, J. Kepler, and P. Zimprich, *Technisches Messen.* **73**, 26 (2006).
14. T. R. Hillman, S. G. Adie, V. Seemann, J. Armstrong, S. L. Jacques, and D. D. Sampson, *Opt. Lett.* **31**, 190 (2006).
15. L. Cuthbert and V. M. Huynh, *Meas. Sci. Technol.* **3**, 740 (1992).
16. K. W. Gossage, C. M. Smith, E. M. Kanter, L. P. Hariri, A. L. Stone, J. J. Rodriguez, S. K. Williams, and J. K. Barton, *Phys. Med. Biol.* **51**, 1563 (2006).
17. M. Asmad, G. Baldwin, C. Maczeyzik, F. Mendoza, and C. P. López, *Proc. SPIE- Int. Soc. Opt. Eng.* **5776**, 530 (2005).
18. B. Horvath, *Optik* **117**, 177 (2006).